https://doi.org/10.5194/tc-2020-222
Preprint. Discussion started: 18 August 2020

The Cryosphere Discussions
Open Access
EGU

A lead-width distribution for Antarctic sea ice: a case study for the Weddell Sea with high resolution Sentinel-2 images

Marek Muchow[1], Amelie U. Schmitt[2], and Lars Kaleschke[3]

[1]Universität Hamburg, Bundesstr. 53, 20146 Hamburg, GERMANY
[2]Universität Hamburg, Bundesstr. 55, 20146 Hamburg, GERMANY
[3]Alfred-Wegener-Institut, Postfach 12 01 61, 27515 Bremerhaven, GERMANY

Correspondence: Marek Muchow (fmnv468@uni-hamburg.de)

Abstract. We derive for the first time a statistical lead-width distribution for Antarctic sea ice using Weddell sea ice as a case study. Therefore, we transfer previous approaches for Arctic sea ice with a power law with a positive exponent ($p(x_{width})\ x_{width}^{-\alpha}, \alpha > 1$) to Antarctic sea ice. We use 20 carefully selected cloud-free Copernicus Sentinel-2 images from November 2016 until February 2018, covering only the months from November to April. In doing so we compare exponents given in the literature for the Arctic sea ice, who do not agree with each other, to Antarctic sea ice.

To detect leads we create a sea ice surface type classification for the Sentinel-2 Level 1C data products, which are selected due to their high spatial resolution of 10 m. We apply two different fitting methods to the measured lead widths, which have been used in previous studies for Arctic sea ice. The first fitting method is a linear fit, while the second method is based on a maximum likelihood approach. Here, we use both methods for the same lead-width data set to observe differences in the calculated power law exponent.

To further investigate influences on the power law exponent, we define two different lead thresholds for open water and nilas. The influence of the lead threshold on the exponent is bigger for the linear fit than for the method based on the maximum likelihood approach. We show that the exponent of the lead-width distribution ranges between 1.16 to 1.41 depending on the applied fitting method and lead threshold. This exponent for the Weddell sea ice is smaller than the previously observed exponents for the Arctic sea ice.

1 Introduction

Leads are created by dynamic motions of the sea ice (Miles and Barry, 1998) and thus follow a linear-like shape. They can be up to tens of kilometers long and are by definition a few meters to some kilometers wide (Alam and Curry, 1997). For parametrization of the lead width lead-width distributions are used. Although there are several lead-width distributions for the Arctic sea ice, there is no lead-width distribution for Antarctic sea ice. We introduce a lead-width distribution for the Weddell sea ice as a case study for Antarctic sea ice.

https://doi.org/10.5194/tc-2020-222
Preprint. Discussion started: 18 August 2020

An adequate representation of leads in coupled climate models is important for various processes. Leads play a large role in the absorption of shortwave radiation due to the low albedo of open water and nilas, compared to the higher albedo of thicker ice and snow covered sea ice (Perovich, 1996). Newly formed leads are also an important area for ice production and the associated brine rejection to the ocean below (Alam and Curry, 1997).

Furthermore, the heat exchange between atmosphere and ocean is strongly enhanced over leads. Maykut (1978) found that the heat loss over thin ice (0.4 - 0.5 m) is one magnitude larger than over multiyear ice. In a model study, Lüpkes et al. (2008) demonstrated that an increase in the lead fraction area by 1 % during polar night can lead to local air temperature warming of up to 3.5 K. Based on buoy data in the Weddell Sea region combined with a thermodynamic sea ice model, Eisen and Kottmeier (2000) found that leads contribute roughly 30 % to the total energy flux from the ocean to the atmosphere in winter months. Due to the large temperature differences between the air and the lead surface in winter, convective plumes forming over leads can have a large impact on the atmospheric processes in regions covered with sea ice (e.g. Tetzlaff et al., 2015; Lüpkes et al., 2008; Chechin et al., 2019).

While using a fetch-dependent formulation of the heat exchange, Marcq and Weiss (2012) demonstrated that the heat transfer is two times more effective for narrow leads of several meters than for wider ones of several hundreds of meters. Furthermore, Qu et al. (2019) found that small leads ($\leq$ 1 km) account for about a quarter of the heat flux over all leads. Reiser et al. (2020) introduced a retrieval algorithm for lead fraction in the Antarctic, but these studies indicate that knowing about lead-width distributions is beneficial when estimating heat transfer.

Shear and divergence rates, estimated from models and satellite observations, follow a power law for the Arctic sea ice (e.g. Girard et al., 2009; Marsan et al., 2004), which suggests that a power law can also be used for the statistical parametrization of the lead width. Indeed, several studies deriving the lead-width distribution for Arctic sea ice from satellite observations found this power law behaviour (e.g. Allison et al., 1993; Marcq and Weiss, 2012; Wernecke and Kaleschke, 2015; Qu et al., 2019). Additionally, in a lead-simulating model by Wang et al. (2016) the total sea ice deformation rate also shows a power law scaling property, which is consistent with observations.

Since different satellite products with different resolutions were used in these studies, there are substantial differences in the methods used to detect leads and of the minimum considered lead widths. Additionally, two different power law fitting methods were applied throughout different studies. The first method is a linear fit (LF method) while the seconds methods is based on a maximum likelihood approach (ML method) after Clauset et al. (2009). Consequently, the results for the power law exponent from satellite observations vary in absolute values and suitable range of the distribution. To narrow down the effect of the fitting method, we applied the two previously used fitting methods to the same data set.

Moreover, all of these previous studies focused on the Arctic and it remains yet to be determined whether the power law approach with the same power law exponents is applicable for Antarctic sea ice leads. The goal of this study is to determine an exponent to describe the width of Antarctic sea ice leads under the assumption that the distribution follows a power law. For this purpose, we analyze Sentinel-2 satellite data for the Weddell Sea as a case study for Antarctic sea ice. The main advantage of the recently launched Sentinel-2 satellites is their high resolution up to 10 m. This enables us to detect also very narrow leads, which former studies were not capable of except the analysis of only one SPOT image by Marcq and Weiss (2012). We use

https://doi.org/10.5194/tc-2020-222
Preprint. Discussion started: 18 August 2020

The Cryosphere Discussions
Open Access
EGU

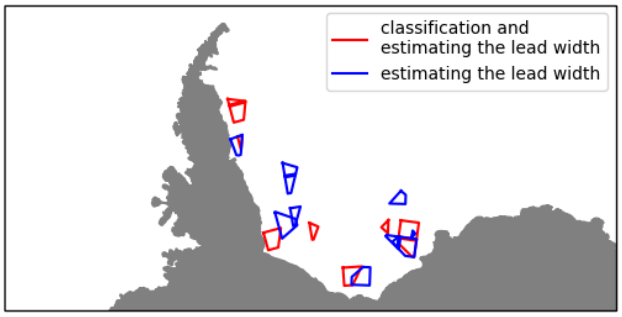

Figure 1. The location of the 20 different Sentinel-2 Level-1C products for this study is the Weddell Sea. Nine out of the 20 were used for the sea ice surface type classification (red border), while for the lead-width detection all 20 were used (red and blue border). Displayed in gray is Antarctic continent border with shelf ice border measured with Satellite Radar from 2007 - 2009 (Rignot et al., 2013).

cloud-free Sentinel-2 Level-1C products, which give the top-of-the-atmosphere (TOA) reflectance (Drusch et al., 2012). The data is described in Section 2. Similar to the albedo for young, thin sea ice the TOA reflectance is related to the ice thickness. We introduce a surface type classification for the Sentinel-2 satellite products to make the data suitable for observing different sea ice types and leads (Sect. 3.1). The determined thresholds for leads covered with open water and with nilas are then used to detect leads and a power law is fitted to the resulting lead-width distribution (Sect. 3.2). Two thresholds are applied to identify the effect of lead coverage definition to the result, since different studies name only open water leads or leads covered with thin ice as leads. The results are presented and discussed in Section 4, followed by conclusions in Section 5.

2 Data

The two sun synchronous Sentinel-2 satellites carry the passively working Multi Spectral Instrument (MSI) with 13 different spectral bands from 443 nm (visible) to 2190 nm (short wave infra-red) (ESA, 2018). The spatial resolution for the bands is either 10, 20 or 60 m while the images cover an area of $100 \times 100\,\mathrm{km}$. For this study images from band 4 are used, due to the fact that they provide the highest spatial resolution with 10 m and show the best representation of the thin ice structures.
The local overpass time of the two Sentinel-2 satellites matches the SPOT satellite and is close to Landsat, which provides the possibility for a future combination the data sets to longer time series. The mission lifetime for Sentinel-2 satellites, which were launched in 2015 and 2017, is planned to be 15 years (Drusch et al., 2012).
For the simplification of the problem only cloud-free Level-1C products were used. Therefore, only products classified as cloud-free were selected in the Copernicus Open Access Hub (https://scihub.copernicus.eu/dhus/#/home). While looking for suitable Sentinel-2 Level-1C products we noticed that on products with wide leads often small clouds occur, most likely from moisture and heat flux through the lead. Those images were rejected manually. We only use totally cloud-free images.
This is a case study for Antarctic sea ice using the Weddell Sea as a study region. It is based on 20 Sentinel-2 Level-1C products taken from November 2016 until February 2018 (Figure 1), covering only the months from November to April due to the need

https://doi.org/10.5194/tc-2020-222
Preprint. Discussion started: 18 August 2020

for sunlight to capture suitable data.

The lead-width detection method (Sect. 3.2) is applied to all 20 products. The classification of surface types (Sect. 3.1) is based on 9 of those 20 products. They cover the time from January to April 2017. For more details on the data see table A1.

3 Methods

3.1 Classification of surface types

The goal of the classification is to get thresholds for different surface types, which include open water and four different ice types (nilas, dark-gray sea ice, light-gray sea ice and sea ice covered with snow). Therefore, nine out of 20 later used Sentinel-2 Level-1C products are utilized (Sect. 2).

On every band 4 image ten areas of each surface type are masked manually. Thereafter, the TOA reflectance of each pixel within the mask is used to create a reflectance value data set for each surface type. The reflectance values lie between zero and one.

To analyze the range of the reflectance for each surface type, histograms are created, which show the occurrence of pixels with a specific TOA reflectance. These histograms are used to fit a summation over Gaussian functions with a weighting parameter a_i to the data:

$$y(x) = \sum_{i=1}^{n} a_i \cdot \frac{1}{\sqrt{2\pi}\sigma_i} \cdot e^{-0.5(\frac{x-\mu_i}{\sigma_i})^2} \tag{1}$$

The Gaussian curve itself has two free parameters: The mean μ and the standard deviation σ. We fit one Gaussian curve ($n = 1$) to the data for open water, nilas and sea ice covered with snow. Respectively, equation 1 with $n = 2$ is used for light-gray sea ice and with $n = 3$ for dark-gray sea ice (Figure 2).

The threshold for each surface category are then determined as the values of the TOA reflectance at the point of intersection of two curves adjacent to each other. An exception is the threshold for open water, where two points of intersection occur. In this case the second point of intersection is chosen to be the threshold, because the first point of intersection is before the maximum. The area of intersection of two curves is then the error of misclassification, also called overlay error, of those thresholds.

To observe the effect of the coverage of the lead we use two TOA reflectance thresholds for determining leads. With the same approach Marcq and Weiss (2012) found different lead-width distribution power law exponents for each threshold.

3.2 Measuring the apparent lead width and determining the power law exponent

The thresholds found with the method in Section 3.1 can be used to classify the Sentinel-2 Level-1C products into binary images. Figure 3 shows examples for the nilas threshold.

Since the leads within each image can have arbitrary orientations, it is difficult to measure lead width orthogonally to the leads orientation. As in Wernecke and Kaleschke (2015) we use the apparent lead width as a proxy for the true lead width. To

https://doi.org/10.5194/tc-2020-222
Preprint. Discussion started: 18 August 2020

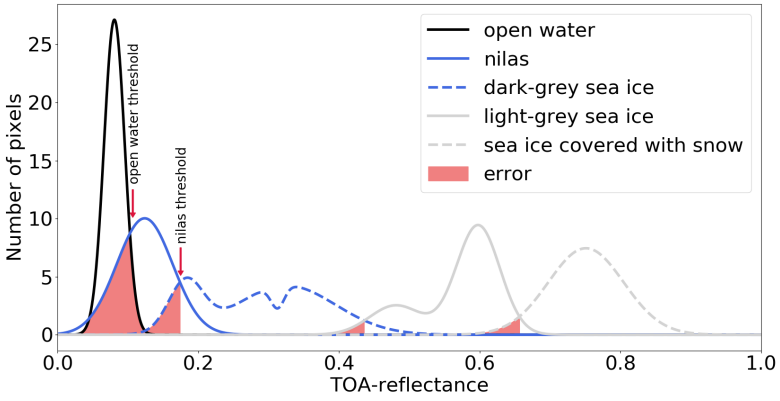

Figure 2. The graphs show the number of pixels within every surface type for a specific TOA reflectance. The fitted Gaussian curves for the frequency of each TOA reflectance for the five different surface ice types are shown. The TOA reflectance threshold for each surface type is the point of intersection of two curves adjacent to each other. The misclassification error is shown as the overlay area of these two curves.

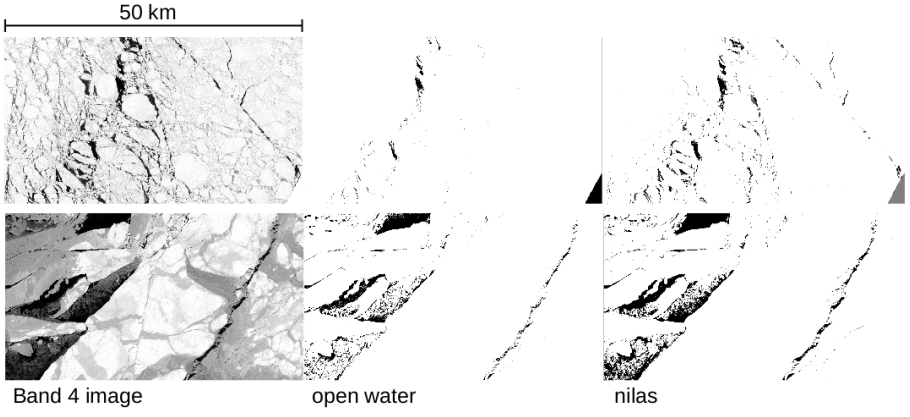

Figure 3. Two example areas of Sentinel-2 Level-1C band 4 images are displayed on the left (sensing date top: 23.02.2017, bottom: 16.03.2017). The upper border of every image is 50 km wide.
The images in the middle are for the open water threshold and the right images for the nilas threshold. Leads are always indicated with black pixels and no leads with white ones. The swath does not cover the whole image area. Thus, only the area covered by the satellite swath is considered for the lead-width measurement.

measure the apparent lead width we use vertical and horizontal measurement tracks with a distance of 10 km to each other. With a data set of the occurrence of the apparent lead widths $p(x)$ it is possible to create a histogram showing the number of leads for each specific width. The assumption is, that the shape of the histogram follows a power law with the exponent α and

https://doi.org/10.5194/tc-2020-222
Preprint. Discussion started: 18 August 2020

the apparent lead widths x_{width}:

$$p(x) = C \cdot x_{width}^{-\alpha} \tag{2}$$

The scaling parameter C is not further investigated. We apply two different methods to estimate the power law exponent α.

For the linear fit (LF method) the apparent lead widths are sorted by size, so that the frequency $p(x)$ of the specific width is available. On a plot with both logarithmic axes, the distribution of the data follows a straight line with specific slope and an axis intercept. The slope is the representation of the power law exponent α. Due to the same influence of every value for the result of the fit, atypical values have a strong effect on the result (Berk, 2004).

The second method for estimating the exponent α is the method for discrete values by Clauset et al. (2009), which is based on a maximum likelihood approach (ML method). The power law distribution diverges at zero, therefore a lower boundary $x_{min} > 0$ is needed. In this study, x_{min} is the smallest possible apparent lead width, which is the image resolution of 10 m. The following equation is used for estimating the power law exponent α:

$$\alpha \approxeq 1 + n \cdot \left[\sum_{i=1}^{n} \ln \left(\frac{x_{width,i}}{x_{min} - \frac{1}{2} \cdot step\ size} \right) \right]^{-1} \tag{3}$$

The total number of counted leads is n, and $x_{width,i}$ are the measured lead widths. Since the data are discrete, 10 m were added to equation 3 as a representation of the step size of the data similar to Wernecke and Kaleschke (2015).

4 Results and discussion

4.1 Classification of surface types

The thresholds between surface categories and corresponding overlap errors is determined using the method described in Section 3.1. With Sentinel-2 band 4 images it is possible to distinguish between five different surface types (Table 1).

The common value used to compare optical properties of sea ice is the albedo. In this study, we measure TOA reflectance instead of albedo. Both properties increase with the sea ice and snow cover thickness, especially for young, thin sea ice in absence of melting processes. In addition to this, the TOA reflectance is only measured passively in the absence of clouds and with a approximately clear atmosphere. Thus, the atmosphere has a neglectable influence on the reflectance measurement. Thus, to evaluate the thresholds for the surface types they are compared to measured albedo values from the East Antarctic sea ice zone in Australian spring and summer by Brandt et al. (2005). Their estimated albedos for open water (0.07) and nilas without snow cover (0.14) are close to the thresholds estimated here for the same surface types. For the classification we aimed to classify structures without snow cover. For the other surface types it is much more difficult to make assumptions about the snow cover or thickness, due to the fact that only the reflectance values are known. Nevertheless, our estimated TOA reflectance thresholds for each surface type is always in the range of the reference albedo measurements from Brandt et al. (2005).

To sum it up, the TOA reflectance thresholds (0.10 for open water and 0.16 for nilas) for the two lead thresholds, which were used for the lead detection, agree with values from previous measurements.

https://doi.org/10.5194/tc-2020-222
Preprint. Discussion started: 18 August 2020

Table 1. The tables displays the threshold for each surface type from the surface classification explained in Section 3.1. Every threshold contains the surface types, which are above it in the table. Sea ice covered with snow has no estimated threshold, therefore it is indicated as 1.0.

Surface type	Threshold [TOA reflectance]	Overlap error [%]
open water	0.10	
		29
nilas	0.17	
		11
dark-gray sea ice	0.44	
		3
light-gray sea ice	0.66	
		4
sea ice covered with snow	1.0	

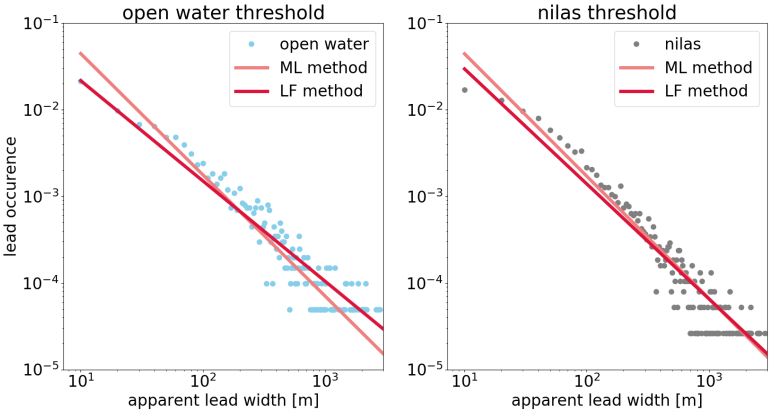

Figure 4. To compare the influence of the applied fitting method, the ML method and LF method were applied for the same data set (open water threshold and nilas threshold) separately. The relative lead occurrence as a function of measured lead width is displayed with gray and blue dots. The straight lines are the fits for each methods.

4.2 Method comparison: Measured lead widths and the power law exponent

Looking at the distribution of the measured lead widths it is evident that the small leads dominate and that with an increasing width the amount of leads decreases. The largest observed apparent lead widths are 6500 m for open water and 6530 m for the nilas threshold. Due to the fact that the nilas threshold covers not only the open water leads, but also the nilas leads, there are around 1700 more leads observed than for the open water threshold.

Our results for the exponent of the power law are different for both methods and thresholds (Table 2). At first we compare the

https://doi.org/10.5194/tc-2020-222
Preprint. Discussion started: 18 August 2020

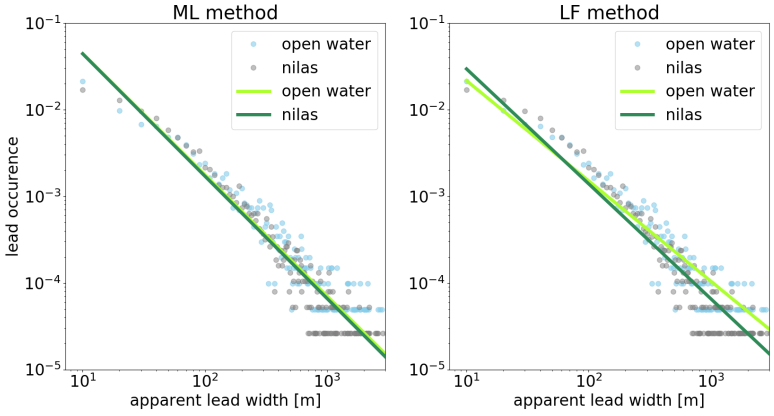

Figure 5. To compare the influence of the applied threshold, the same fitting method (ML or LF method) was applied for the two data sets with different thresholds (open water threshold and nilas threshold) separately. The relative lead occurrence as a function of measured lead width is displayed with gray and blue dots. The straight lines are the fits for each methods.

results for the same thresholds with different methods to one another (Figure 5) to see the effect of the methods. The values for the power law exponent with the open water threshold are 1.16 (LF method) and 1.40 (ML method). In this case this method has a strong implication on the result. For the nilas threshold the results are closer (LF method: 1.33, ML method: 1.41), but not within the same range if their standard deviation is applied. The standard deviation for the LF method is four times higher (0.04) than for the ML method (0.01). That confirms that the method has a non neglectable effect on the result of the exponent for the sea ice width distribution power law.

Secondly, we compare the results for the same method with different thresholds to show the importance of the choice of thresholds (Figure 4). The open water threshold covers only leads without any thin sea ice, while the nilas threshold includes open water but also thin sea ice structures. Thus, the nilas threshold data set includes more lead-width measurements but also wider leads. For the LF method the different thresholds gives two different results of the exponent for the sea ice width distribution power law (open water: 1.16, nilas: 1.33). Otherwise, for the ML method the choice of the threshold has no influence within the range of the standard deviation for the result of the power law exponent (open water: 1.40, nilas: 1.41). Choosing different thresholds or criteria for the definition of the lead can influence the result. This is supported by the result of Marcq and Weiss (2012), who used two differing thresholds which have a similar range to one another as our estimates for the LF method (Table 2).

Based on our current knowledge, previous studies (Table 2) focused on different regions in the Arctic and not on Antarctic regions. Comparing the results of this study with previous studies it is clear that the results for the exponent of the power law for the Weddell Sea are smaller than the ones for the Arctic sea ice. The results by Wernecke and Kaleschke (2015) using the CryoSat-2 satellite support the earlier mentioned results by Marcq and Weiss (2012) (SPOT satellite) with a power law exponent around 2.50. The power law exponent found by Qu et al. (2019) (2.241 - 2.346) using a combination of MODIS and

https://doi.org/10.5194/tc-2020-222
Preprint. Discussion started: 18 August 2020

Landsat 8 is in the same range as the first and lower exponent from Marcq and Weiss (2012), who also used two thresholds. Furthermore, there were two surveys using submarines from which power law exponents of 2.00 and 2.29 were calculated (Wadhams (1981) and Wadhams et al. (1985)). The only result with an exponent not ranging from 2 to 2.6 is from Lindsay and Rothrock (1995), which has a power law exponent of 1.60. They used data from an Advanced Very High Resolution Radiometer (AVHRR).

The differences between the results could arise from different satellite sensors or methods. For example, different definitions of leads or fitting methods influence the lead-width distribution. For future comparison the same fitting method should be applied, since our study shows that with the same data different results occur.

Furthermore, the results for the power law exponent displayed in Table 2 are based on a scale invariant approach, while Qu et al. (2019) used different resolutions of the measured lead width ranging from $30\,\mathrm{m}$ to $1\,\mathrm{km}$ resulting in differences in the power law exponent in the first decimal place. In addition to that Rampal et al. (2019) confirmed a multi-fractal dependence of the sea ice deformation rates on time and space scales. Thus, applying these results on different processes related to deformation, like leads formed due to divergence, would be a necessary step for further research.

Another possible reason for the differences are the different conditions in both regions. While the Arctic Ocean is surrounded by land mass, the Southern Ocean is around the Antarctic Continent. The Antarctic sea ice is exposed to the Antarctic Circumpolar Current and strong circumpolar winds. The Antarctic sea-ice cover is generally more divergent than much of the Arctic ice cover (Gloersen et al., 1993). Worby et al. (2008) estimated the long-term mean (1981 - 2005) of total Antarctic sea ice thickness in winter as $0.66 \pm 0.60\,\mathrm{m}$. For the Arctic Ocean, Kwok et al. (2009) calculated a 5-year mean (2003 - 2008) ice thickness during winter of $2.9 \pm 0.3\,\mathrm{m}$. Different sea ice thicknesses influence the sea ice to have different rheologic properties (Feltham, 2008). Thus, it is necessary to do further research on leads in the Southern Ocean to fully understand differences and similarities between the Arctic and Antarctic sea ice.

4.3 Availability of Sentinel-2 for observing leads

The resolution of the Sentinel-2 satellites is higher compared to the satellite data used in previous studies, except for the SPOT satellite used by Marcq and Weiss (2012) (Table 2). Thus, the resolution of the different observed widths is higher, but also the power law starts at a smaller scale.

While the Sentinel-2 satellites offer a high resolution of $10\,\mathrm{m}$ in the visible wave length range, there are also disadvantages with this set up for observing leads. The amount of available data in sea ice regions decreases drastically if only cloud-free data are used. The upper limit of the power law range is cut off by the availability of wider leads, since wider leads tend to produce small clouds. During our whole analysis period every used product needed to be manually checked for clouds, due to a not completely accurate classification by the provider, the Copernicus Open Access Hub.

Due to the fact that leads normally have sharp edges the selection of areas as example values for open water and nilas was comparably easy. The thicker the ice and snow cover the more unreliable these observations become. To obtain a more precise classification of the surface types validation with other data sources could be beneficial.

https://doi.org/10.5194/tc-2020-222
Preprint. Discussion started: 18 August 2020

Table 2. The table shows different results for the power law exponent sorted by publishing date. The last two entries are the results of this work for the Weddell sea. Marcq and Weiss (2012) use two different thresholds, that is why they have two results.
LF method stands for a linear fit and ML method stays for the method after Clauset et al. (2009). A detailed explanation of the methods is in Section 3.2

Source	Fitting method	Platform/ Instrument	Time and region	Resolution of the power law	Range of the power law	Power law exponent α
Wadhams (1981)	LF	submarine mission	October 1976, European Arctic Ocean	about 5 m	50 - 1000 m	2.00
Wadhams et al. (1985)	LF	submarine mission	February 1967, Davis Strait	about 5 m	50 - 1000 m	2.29
Lindsay and Rothrock (1995)	LF	AVHRR	1989, Central Arctic Ocean	1 km	1 - 50 km	1.60 ± 0.18
Marcq and Weiss (2012)	ML	SPOT	April 1996, Central Arctic Ocean	10 m	0.02 - 2 km	2.1 - 2.3 2.5 - 2.6
Wernecke and Kaleschke (2015)	ML	CryoSat-2	winter 2011 - 2014, Arctic Ocean	300 m	≥ 600 m	2.47 ± 0.04
Qu et al. (2019)	LF	MODIS, Landsat-8	April 2015, Beaufort Sea	30 m - 1 km	≥ 30 m	2.241 - 2.346
this study	LF	Sentinel-2	2016 - 2018 (Nov - Apr), Weddell Sea	10 m	0.01 - 6.5 km	1.16 ± 0.04 1.33 ± 0.04
this study	ML	Sentinel-2	2016 - 2018 (Nov - Apr), Weddell Sea	10 m	0.01 - 6.5 km	1.40 ± 0.01 1.41 ± 0.01

Regardless of the displayed difficulties, Sentinel-2 data is a suitable, high-resolution complement to remote sensing based research and observation of sea ice and leads.

https://doi.org/10.5194/tc-2020-222
Preprint. Discussion started: 18 August 2020

5 Conclusions

We introduce for the first time a lead-width distribution for Antarctic sea ice using Weddell sea ice as a case study. We confirm that the lead-width distribution for Weddell sea ice follows a power law, showing similar behavior to the lead-width distribution in the Arctic (Wadhams, 1981; Wadhams et al., 1985; Lindsay and Rothrock, 1995; Marcq and Weiss, 2012; Wernecke and Kaleschke, 2015; Qu et al., 2019), but with a smaller exponent.

We apply two different fitting methods to the measured lead widths, which have been used in previous studies for Arctic sea ice (Wadhams, 1981; Wadhams et al., 1985; Lindsay and Rothrock, 1995; Marcq and Weiss, 2012; Wernecke and Kaleschke, 2015). The first fitting method is a linear fit (LF method), while the second method is based on a maximum likelihood approach by Clauset et al. (2009) (ML method). To further investigate influences on the power law exponent, we define two different lead thresholds for open water and for nilas. To observe leads with Sentinel-2 Level 1C products, it is necessary to have a surface type classification. Therefore we created a surface type classification based on the top-of-the-atmosphere (TOA) reflectance. For open water the TOA reflectance threshold is 0.10 with a missclassification error of 29 %, while the threshold for nilas is 0.17 with a missclassification error of 11 %. The threshold for nilas includes also open water leads. With this classification the Sentinel-2 Level 1C data can be used to detect and observe sea ice leads under cloud-free conditions with a resolution of 10 m. We demonstrate that the fitting method has an influence on the result of the exponent and for further investigations, established methods should be applied to guarantee comparability of the results. With the LF method the power law exponent for the lead-width distribution is 1.16 - 1.33 including both lead thresholds, while the exponent with the ML method shows less dependence on the threshold and is 1.40 - 1.41.

Data availability. Analysed Sentinel-2 Level-1C products

All used Sentinel-2 Level-1C products are displayed in Table A1. We accessed the data using the Copernicus Open Access Hub (https://scihub.copernicus.eu/dhus/#/home).

Author contributions. MM acquired and checked the data, created the surface type classification and derived the lead-width distribution under the supervision of LK. AS helped with the derivation of the lead width distribution and editing the paper. MM prepared the paper with contributions of all co-authors.

Competing interests. The authors declare that they have no conflict of interest.

https://doi.org/10.5194/tc-2020-222
Preprint. Discussion started: 18 August 2020


The Cryosphere Discussions
Open Access
EGU

Table A1. Sentinel-2 Level-1C products used for classification (labeled with yes) and for measuring the lead width (all).

Sensing date	Classification	Product name
12/11/2016	no	S2A_MSIL1C_20161112T104212_N0204_R122_T26CMC_20161112T104210
20/11/2016	no	S2A_MSIL1C_20161120T100152_N0204_R093_T25CES_20161120T100153
20/11/2016	no	S2A_MSIL1C_20161120T100152_N0204_R093_T25CDS_20161120T100153
29/11/2016	no	S2A_MSIL1C_20161129T103152_N0204_R079_T24CXE_20161129T103151
20/12/2016	no	S2A_MSIL1C_20161220T100052_N0204_R093_T24CVV_20161220T100049
23/02/2017	yes	S2A_MSIL1C_20170223T123141_N0204_R023_T21CVT_20170223T123144
23/02/2017	no	S2A_MSIL1C_20170223T123141_N0204_R023_T22DDF_20170223T123144
23/02/2017	no	S2A_MSIL1C_20170223T123141_N0204_R023_T22DDG_20170223T123144
24/02/2017	yes	S2A_MSIL1C_20170224T120231_N0204_R037_T22CEC_20170224T120234
26/02/2017	yes	S2A_MSIL1C_20170226T110241_N0204_R065_T23CNQ_20170226T110244
02/03/2017	no	S2A_MSIL1C_20170302T122211_N0204_R123_T22CDD_20170302T122205
13/03/2017	no	S2A_MSIL1C_20170313T101141_N0204_R136_T25CDS_20170313T101144
16/03/2017	yes	S2A_MSIL1C_20170316T102141_N0204_R036_T25CES_20170316T102141
16/03/2017	yes	S2A_MSIL1C_20170316T102141_N0204_R036_T25CES_20170316T102141
16/03/2017	yes	S2A_MSIL1C_20170316T102141_N0204_R036_T24CWC_20170316T102141
06/04/2017	yes	S2A_MSIL1C_20170406T131051_N0204_R052_T21DVF_20170406T131050
06/04/2017	yes	S2A_MSIL1C_20170406T131051_N0204_R052_T21DVG_20170406T131050
06/04/2017	yes	S2A_MSIL1C_20170406T131051_N0204_R052_T21DVD_20170406T131050
06/04/2017	no	S2A_MSIL1C_20170406T131051_N0204_R052_T20DPJ_20170406T131050
09/02/2018	no	S2A_MSIL1C_20180209T120241_N0206_R037_T21CWU_20180209T163245

Acknowledgements. This work was financially supported by the German Science Foundation (DFG) with the project number 314651818. The authors acknowledge the Copernicus program and the European space agency (ESA) for providing the imagery data for the Sentinel-2 satellites with the Copernicus Open Access Hub.

https://doi.org/10.5194/tc-2020-222
Preprint. Discussion started: 18 August 2020

References

Alam, A. and Curry, J. A.: Determination of surface turbulent fluxes over leads in Arctic sea ice, Journal of Geophysical Research: Oceans, 102, 3331–3343, https://doi.org/10.1029/96JC03606, 1997.

Allison, I., Brandt, R. E., and Warren, S. G.: East Antarctic sea ice: Albedo, thickness distribution, and snow cover, Journal of Geophysical Research: Oceans, 98, 12 417–12 429, https://doi.org/10.1029/93JC00648, 1993.

Berk, R. A.: Regression analysis: A constructive critique, vol. 11, Sage, 2004.

Brandt, R. E., Warren, S. G., Worby, A. P., and Grenfell, T. C.: Surface albedo of the Antarctic sea ice zone, Journal of Climate, 18, 3606–3622, https://doi.org/10.1175/JCLI3489.1, 2005.

Chechin, D. G., Makhotina, I. A., Lüpkes, C., and Makshtas, A. P.: Effect of wind speed and leads on clear-sky cooling over Arctic sea ice during polar night, Journal of the Atmospheric Sciences, 76, 2481–2503, https://doi.org/10.1175/JAS-D-18-0277.1, 2019.

Clauset, A., Shalizi, C. R., and Newman, M. E.: Power-law distributions in empirical data, SIAM review, 51, 661–703, https://doi.org/10.1137/070710111, 2009.

Drusch, M., Del Bello, U., Carlier, S., Colin, O., Fernandez, V., Gascon, F., Hoersch, B., Isola, C., Laberinti, P., Martimort, P., et al.: Sentinel-2: ESA's optical high-resolution mission for GMES operational services, Remote sensing of Environment, 120, 25–36, https://doi.org/10.1016/j.rse.2011.11.026, 2012.

Eisen, O. and Kottmeier, C.: On the importance of leads in sea ice to the energy balance and ice formation in the Weddell Sea, Journal of Geophysical Research: Oceans, 105, 14 045–14 060, https://doi.org/10.1029/2000JC900050, 2000.

ESA: sentinel online, available at https://earth.esa.int/web/sentinel/user-guides/sentinel-2-msi/resolutions/spatial, last access: 19/09/2019, 2018.

Feltham, D. L.: Sea ice rheology, Annu. Rev. Fluid Mech., 40, 91–112, https://doi.org/10.1146/annurev.fluid.40.111406.102151, 2008.

Girard, L., Weiss, J., Molines, J.-M., Barnier, B., and Bouillon, S.: Evaluation of high-resolution sea ice models on the basis of statistical and scaling properties of Arctic sea ice drift and deformation, Journal of Geophysical Research: Oceans, 114, https://doi.org/10.1029/2008JC005182, 2009.

Gloersen, P., Campbell, W. J., Cavalieri, D. J., Comiso, J. C., Parkinson, C. L., and Zwally, H. J.: Satellite passive microwave observations and analysis of Arctic and Antarctic sea ice, 1978–1987, Annals of Glaciology, 17, 149–154, https://doi.org/10.3189/S0260305500012751, 1993.

Kwok, R., Cunningham, G., Wensnahan, M., Rigor, I., Zwally, H., and Yi, D.: Thinning and volume loss of the Arctic Ocean sea ice cover: 2003–2008, Journal of Geophysical Research: Oceans, 114, https://doi.org/10.1029/2009JC005312, 2009.

Lindsay, R. and Rothrock, D.: Arctic sea ice leads from advanced very high resolution radiometer images, Journal of Geophysical Research: Oceans, 100, 4533–4544, https://doi.org/10.1029/94JC02393, 1995.

Lüpkes, C., Vihma, T., Birnbaum, G., and Wacker, U.: Influence of leads in sea ice on the temperature of the atmospheric boundary layer during polar night, Geophysical Research Letters, 35, https://doi.org/10.1029/2007GL032461, 2008.

Marcq, S. and Weiss, J.: Influence of sea ice lead-width distribution on turbulent heat transfer between the ocean and the atmosphere, The Cryosphere, 6, 143–156, https://doi.org/10.5194/tc-6-143-2012, 2012.

Marsan, D., Stern, H., Lindsay, R., and Weiss, J.: Scale dependence and localization of the deformation of Arctic sea ice, Physical review letters, 93, 178 501, https://doi.org/10.1103/PhysRevLett.93.178501, 2004.

https://doi.org/10.5194/tc-2020-222
Preprint. Discussion started: 18 August 2020

Maykut, G. A.: Energy exchange over young sea ice in the central Arctic, Journal of Geophysical Research: Oceans, 83, 3646–3658, https://doi.org/10.1029/JC083iC07p03646, 1978.

Miles, M. W. and Barry, R. G.: A 5-year satellite climatology of winter sea ice leads in the western Arctic, Journal of Geophysical Research: Oceans, 103, 21 723–21 734, https://doi.org/10.1029/98JC01997, 1998.

Perovich, D. K.: The optical properties of sea ice, Tech. rep., COLD REGIONS RESEARCH AND ENGINEERING LAB HANOVER NH, 1996.

Qu, M., Pang, X., Zhao, X., Zhang, J., Ji, Q., and Fan, P.: Estimation of turbulent heat flux over leads using satellite thermal images, The Cryosphere, 13, 1565–1582, https://doi.org/10.5194/tc-13-1565-2019, 2019.

Rampal, P., Dansereau, V., Olason, E., Bouillon, S., Williams, T., Korosov, A., and Samaké, A.: On the multi-fractal scaling properties of sea ice deformation, The Cryosphere, 13, 2457–2474, 2019.

Reiser, F., Willmes, S., and Heinemann, G.: A New Algorithm for Daily Sea Ice Lead Identification in the Arctic and Antarctic Winter from Thermal-Infrared Satellite Imagery, Remote Sensing, 12, 1957, 2020.

Rignot, E., Jacobs, S., Mouginot, J., and Scheuchl, B.: Ice-shelf melting around Antarctica, Science, 341, 266–270, https://doi.org/10.1126/science.1235798, 2013.

Tetzlaff, A., Lüpkes, C., and Hartmann, J.: Aircraft-based observations of atmospheric boundary-layer modification over Arctic leads, Quarterly Journal of the Royal Meteorological Society, 141, 2839–2856, https://doi.org/10.1002/qj.2568, 2015.

Wadhams, P.: Sea-ice topography of the Arctic Ocean in the region 70 W to 25 E, Phil. Trans. R. Soc. Lond. A, 302, 45–85, https://doi.org/10.1098/rsta.1981.0157, 1981.

Wadhams, P., McLaren, A. S., and Weintraub, R.: Ice thickness distribution in Davis Strait in February from submarine sonar profiles, Journal of Geophysical Research: Oceans, 90, 1069–1077, https://doi.org/10.1029/JC090iC01p01069, 1985.

Wang, Q., Danilov, S., Jung, T., Kaleschke, L., and Wernecke, A.: Sea ice leads in the Arctic Ocean: Model assessment, interannual variability and trends, Geophysical Research Letters, 43, 7019–7027, https://doi.org/10.1002/2016GL068696, 2016.

Wernecke, A. and Kaleschke, L.: Lead detection in Arctic sea ice from CryoSat-2: quality assessment, lead area fraction and width distribution, The Cryosphere, 9, 1955–1968, https://doi.org/10.5194/tc-9-1955-2015, 2015.

Worby, A. P., Geiger, C. A., Paget, M. J., Van Woert, M. L., Ackley, S. F., and DeLiberty, T. L.: Thickness distribution of Antarctic sea ice, Journal of Geophysical Research: Oceans, 113, https://doi.org/10.1029/2007JC004254, 2008.